An Eight-Channel Hyperfine Wavelength Demultiplexer Using a Virtually Imaged Phased-Array (VIPA)

Shijun Xiao, *Student Member, IEEE,* and Andrew M. Weiner, *Fellow, IEEE*

***Abstract*—We demonstrate an eight-channel hyperfine wavelength demultiplexer at 1.55 μm using a virtually imaged phased-array spectral disperser, with channel spacings of $\sim$3 GHz (24 pm) and $-$3-dB channel bandwidths of $\sim$0.75 GHz (6 pm). We achieve adjacent channel isolations $\geq$23 dB and nonadjacent channel isolations $\geq$30 dB. We also present the first theoretical analysis.**

***Index Terms*—Hyperfine wavelength-division multiplexing (WDM), ultradense wavelength-division multiplexing (WDM), wavelength demultiplexers.**

TECHNOLOGY for separating and combining wavelengths is fundamental to wavelength-division multiplexing (WDM). Multiplexing–demultiplexing devices with substantially finer spectral resolutions could lead to new opportunities for networks with finer wavelength granularities and larger channel counts, as well as new possibilities for optical signal processing. The well-known arrayed waveguide grating technology channel spacing is limited to 10 GHz [1]. Technology based on a modified side-entrance Fabry–Pérot etalon termed a virtually imaged phased-array (VIPA) [2], [3] shows strong potential for hyperfine WDM multiplexing–demultiplexing. Such hyperfine WDM technology has been used to separate spectral lines from a 12.4-GHz mode-locked laser for applications in photonic arbitrary waveform generation [4] and from a 10-GHz mode-locked laser in order to demonstrate laser repetition rate multiplication [5]. VIPAs have also been used in a Fourier transform pulse shaper geometry [6] to implement novel dispersion compensation systems based on optical signal processing [7]. Recently, we used a direct space-to-time pulse shaper based on the VIPA to demonstrate microwave arbitrary waveform generation with $\sim$1-ns time aperture [8]. We also demonstrated demultiplexing spectra from a VIPA with a 3-dB linewidth below 10 pm (1.25 GHz) [9], where we focused on the narrow filter properties of the VIPA demultiplexer. Here, for the first time in experiments to our knowledge, we report an eight-channel wavelength demultiplexer using the VIPA spectral disperser with $\sim$3-GHz (24 pm) channel spacings and $\sim$0.75-GHz (6 pm) $-$3-dB channel bandwidths. Furthermore, we present the first theoretical discussion.

Manuscript received June 16, 2004; revised August 30, 2004. This work was supported in part by the ARO under Grant DAAD19-03-1-0275.

The authors are with the School of Electrical and Computer Engineering, Purdue University, West Lafayette, IN 47907-1285 USA (e-mail: sxiao@ecn.purdue.edu; amw@ecn.purdue.edu).

Digital Object Identifier 10.1109/LPT.2004.839017

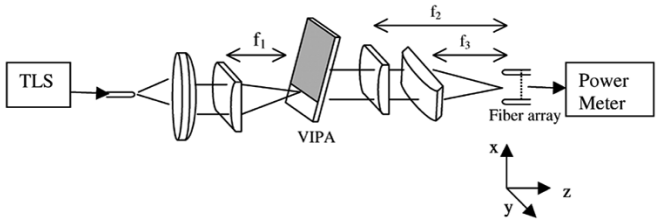

Fig. 1. Experimental setup for our eight-channel hyperfine WDM wavelength demultiplexer.

The VIPA is a relatively new optical spectral disperser based on a "side-entrance" Fabry–Pérot etalon geometry. It typically consists of two glass plates, of which the back or the transmission side is coated with a partially reflective film (e.g., field reflectivity $r \geq 95\%$); the front or entry side is coated with an almost $R \sim 100\%$ reflective film except in a window area, which is uncoated or antireflection coated. If the etalon cavity is filled with air, it is called an air-spaced VIPA; otherwise, if it is filled with some glass of refractive index n_r, it is called a solid VIPA. A collimated beam is focused by a cylindrical lens into the VIPA at a small angle through the window area, and the injected beam experiences multiple reflections between the two plates of the VIPA. The angular dispersion is achieved via the multiple beam interference. An important property of the VIPA is that it can provide significantly larger angular dispersion than typical diffraction gratings.

Fig. 1 shows our setup. A solid $\sim$50-GHz VIPA with some glass of a refractive index $n_r \sim 2$ and a thickness $t\sim$1.5 mm is used. One important difference from our previous setups [9] is that at the output, we use a single-mode fiber (SMF-28) array with eight ports instead of a bare SMF. The adjacent fiber spacing is 127 μm. In addition, we use two cylindrical lenses with a common back focal plane for focusing in the x and y dimensions, respectively, instead of a single spherical lens. This gives us an additional freedom to design the channel spacing while improving the coupling efficiency into output SMFs. The demultiplexer passband shape is measured using a tunable laser source (Agilent 81 680 A), that has a linewidth below 0.1 pm. A power sensor (Agilent 81 632 A) is used to record the output power as the wavelength is swept. Each port of the eight-port fiber array is measured by separate sweeps of the source wavelength at a step size of 1 pm.

Assuming the spectral dispersion is in the x dimension, the intensity distribution on the common back focal plane of the two focusing cylindrical lenses is [9], [10]

$$I_{\text{out}}(x,y,\lambda) \propto |E_{\text{out}}(x,y,\lambda)|^2 \propto \exp\left(-2\frac{\pi^2 W^2 y^2}{f_3^2\lambda^2}\right) \times \exp\left(-2\frac{f_1^2 x^2}{f_2^2 W^2}\right) \frac{1}{(1-Rr)^2 + 4(Rr)\sin^2\left(\frac{k\Delta}{2}\right)} \quad (1)$$

where

$$\Delta = 2tn_r\cos(\theta_{\text{in}}) - 2t\frac{\tan(\theta_{\text{in}})\cos(\theta_i)x}{f_2} - t\frac{\cos(\theta_{\text{in}})x^2}{n_r f_2^2}$$

where f_1, f_2, and f_3 are the focal lengths of the cylindrical lenses (see Fig. 1). θ_i is the beam incident angle into the VIPA, $\theta_{\text{in}} = \theta_i/n_r$ is the internal angle inside the VIPA, W is the beam radius (intensity falls to $1/e^2$ compared to the center) of the collimated input beam prior to cylindrical Lens 1, and $k = 2\pi/\lambda$ is the wave vector in free space. The wavelength spatial dispersion can be expressed by [10]

$$\Delta\lambda(x) = \lambda_p(x) - \lambda_0 = -\lambda_0\left[\frac{\tan(\theta_{\text{in}})\cos(\theta_i)}{n_r\cos(\theta_{\text{in}})}\frac{x}{f_2} + \frac{1}{2}\frac{1}{n_r^2}\frac{x^2}{f_2^2}\right] \quad (2)$$

where $\lambda_p(x)$ is the peak wavelength at position x, and $m\lambda_0 = 2tn_r\cos(\theta_{\text{in}})$, where m is an integer.

Derived from (1), the theoretically minimal -3-dB channel bandwidth in frequency and wavelength units is given, respectively, by

$$\text{FWHM}_{\text{frequency}} = \frac{c}{2\pi n_r t\cos(\theta_i)}\frac{1-Rr}{\sqrt{Rr}}$$
$$\text{FWHM}_{\text{wavelength}} = \frac{\lambda_0^2}{2\pi n_r t\cos(\theta_i)}\frac{1-Rr}{\sqrt{Rr}}. \quad (3)$$

In our case, $\cos(\theta_i) \sim 1, n_r \sim 2$, and $t \sim 1.5$ mm. Considering, for the sake of illustration, a ballpark estimate $Rr = 96\%$, (3) gives an estimated 3-dB channel bandwidth of $\sim$0.65 GHz (5.2 pm at 1.55 μm).

Our main design goal is to specify the numerical values of all the focal lengths in order to implement multiple channels with optimized insertion loss. In order to trap enough reflected beams (>50 back-forth reflections) inside the VIPA with a finite aperture of 7 mm in x, the incident angle should be $\theta_i < 5^\circ$. This accommodates sufficient reflections that we can approach the minimum channel bandwidth and insertion loss. In our experiments, θ_i is $\sim 2^\circ \pm 0.2^\circ$ to make sure of an enough large angular dispersion.

The choice of f_1 must optimize the beam size coupled into the VIPA etalon. With the beam waist located on the transmissive surface, the focused beam waist must satisfy the following equation to make sure of low beam clipping loss at the edge of the window on the input surface

$$t\tan(\theta_i/n_r) \geq w_0\sqrt{1 + \frac{t^2\lambda^2}{n_r^2\pi^2 w_0^4}}.$$

For an incident angle $\theta_i = 2.2^\circ$, this gives 16 μm $\leq w_0 \leq$ 24 μm. According to $w_0 = (f_1\lambda/\pi W)$ ($W = 1.2$ mm is the radius of the collimated input beam), we have 39 mm $\leq f_1 \leq$ 58 mm. In our experiments, we used $f_1 = 60$ mm, which is close to the optimal range. In our case, we estimate a power clipping loss $\sim$4%, which is close to the estimate in [3].

The next task is to specify and design the optimal channel spacing with >20-dB adjacent channel isolation. Our previous measurements on the passband shape of the VIPA demultiplexing filter gave a $\sim$50-pm $-$20-dB channel bandwidth [9], and this means a channel spacing of $\sim$25 pm (3.125 GHz) is possible constrained by the required channel crosstalk >20 dB. With a fixed adjacent fiber spacing 127 μm in a fiber array and an incident angle $\theta_i \sim 2^\circ$, the focal length f_2 can be calculated using the dispersion relation (2). We use $f_2 = 75$ mm. For fixed fiber mode size and fiber-to-fiber spacing, there is a tradeoff between the designed channel spacing and channel bandwidth and the coupling efficiency; as a result, we choose a focused mode size to be several times larger than that in the SMF. In addition, the focused mode has approximately Lorentzian shape, resulting in a further mode mismatch. Our numerical simulation indicates $\sim$7-dB power loss due to the coupling between the focused mode and the fiber mode. In our case, the loss due to diffraction from the VIPA into higher orders is estimated to be $\sim$1 dB, which agrees with the value in [3]. Thus, in our case, we estimate a fundamental insertion loss $\sim$8 dB, assuming optimal beam focusing into the VIPA etalon.

The choice of $f_3 = 10$ mm is determined by the goal of optimal coupling into a SMF in the y direction (nondispersion direction). The SMF (9/125) has a mode radius of $\sim$5 μm (the field intensity decays to $1/e^2$ compared to the center); thus, the f_3 is calculated by $f_3 = \pi W a/\lambda$.

Fig. 2 shows the measured channel response for the channel numbered as 1 (see Fig. 3), which has a $\sim$0.75-GHz (6 pm) $-$3-dB bandwidth and a $\sim$0.5-GHz (4 pm) $-$1-dB bandwidth. Our theory predicts a Lorentzian lineshape for the channel response. For a lineshape comparison shown in Fig. 2, the dashed curve is a Lorentzian lineshape, and the dotted curve is a Gaussian lineshape. The actual lineshape is between a Lorentzian lineshape and a Gaussian lineshape, and the three are very close between the peak and $\sim-$5-dB level below the peak. The actual lineshape deviates from the Lorentzian lineshape at the $-$5-dB level, and it continues to match the Gaussian lineshape until the $-$12-dB level. The observed lineshape rolls off much faster than a Lorentzian lineshape, which is beneficial to obtaining small channel spacings and low channel crosstalk. We attribute these deviations above to the finite mode size of the fiber, which is not accounted for in our theory which assumes a point receiver. We also attribute the ripples on the wings of the channel response to nonideal effects, such as lens aberration, which are resolved by the 1-pm steps in our wavelength sweeps.

Fig. 3 shows the complete characterization of all eight channels implemented on the fiber array with eight ports. The demultiplexer has a 50-GHz (0.4 nm) free-spectral range, which indicates that the channel response has a period of 0.4 nm (corresponding to the diffraction orders shown in Fig. 3). The channel positions can be tuned by changing the beam incident angle θ_i or by translating the fiber array along the x dimension. Complete data for eight channels from one diffraction order are shown in Table I. Curve fitting is used to estimate 1-dB bandwidths since they are only three to four times wider than the 1-pm wavelength step. The insertion losses range from 12 to 13 dB, which are somewhat higher than the theoretical estimate of 8 dB.

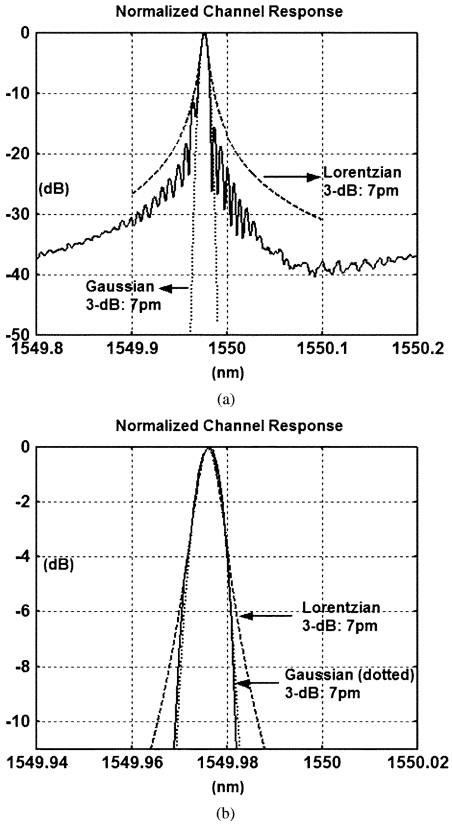

Fig. 2. Lineshape of the response of channel numbered as 1 in Fig. 3. (b) Zoom-in version of (a).

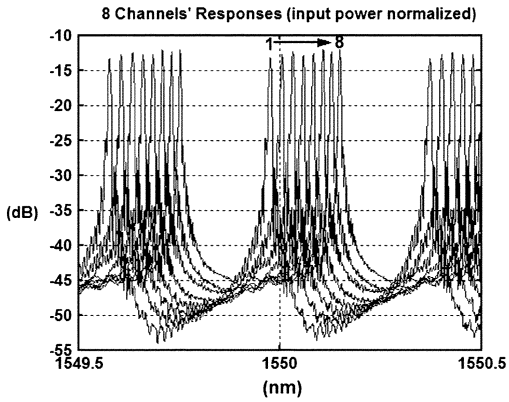

Fig. 3. Responses of all eight channels measured using the fiber array of eight ports: channel spacing ∼3 GHz, −3-dB channel bandwidth ∼0.75 GHz. The numbers from 1 to 8 mark one diffraction order.

The adjacent channel isolation is ≥23 dB, and the nonadjacent channel isolation is ≥30 dB. The variation of angular dispersion with output angle, predicted by (2), results in a variation of the channel spacing. A constant channel spacing would be possible using a fiber array with nonuniform spacing, specified according to the dispersion relation (2). A minimum 3-dB channel bandwidth ∼4.8 pm is obtained in Channel 8. According to (3), this would be in accord with a reflectivity product $Rr \sim 96.2\%$. The variation of 3-dB channel bandwidth across the eight channels is roughly proportional to the variation of angular dispersion and, hence, to the variation in channel spacings.

TABLE I
CHANNEL PARAMETERS FOR ALL EIGHT CHANNELS WITHIN A SINGLE DIFFRACTION ORDER (CORRESPONDING TO THE ORDER NUMBERED FROM 1 TO 8 IN FIG. 3). BANDWIDTH PARAMETERS ARE MEASURED OVER SEVERAL DIFFRACTION ORDERS SHOWN IN FIG. 3; BOTH AVERAGE VALUES AND THE MAGNITUDE OF THE VARIATIONS ARE GIVEN. CHANNEL ISOLATION IS DEFINED AS THE SUPPRESSION OF OTHER CHANNELS IN DECIBELS AT THE CENTER CHANNEL WAVELENGTH OF A DESIRED CHANNEL

Channel #	1	2	3	4	5	6	7	8
1 dB Bandwidth (pm)	4 ± 0.5	4	3.8 ± 0.3	3.3 ± 0.3	3.2 ± 0.3	3	3.3 ± 0.3	2.8 ± 0.3
3 dB Bandwidth (pm)	6.5 ± 0.5	6.5 ± 0.5	6.3 ± 0.3	5.8 ± 0.3	5.5 ± 0.5	5	5.5 ± 0.5	4.8 ± 0.3
Peak-1549(nm)	0.577	0.606	0.634	0.660	0.685	0.708	0.731	0.753
Loss (dB)	13.2	12.8	12.5	12.8	12.7	12.1	12.4	12.1
Spacing (pm)	29 (1-2)		26 (3-4)		23 (5-6)		22 (7-8)	
		28 (2-3)		25 (4-5)		23 (6-7)		
Isolation (dB)	Adjacent ≥ 23 Non-Adjacent ≥ 30							

In summary, we have theoretically discussed the design of an eight-channel hyperfine wavelength demultiplexer implemented by a VIPA spectral disperser and a fiber array receiver. Experimentally, we have demonstrated a hyperfine wavelength demulitplexer with channel spacings ∼3 GHz, ∼0.75 GHz −3-dB bandwidths, insertion losses ranging from 12 to 13 dB, adjacent channel isolations (crosstalk) better than 23 dB, and nonadjacent channel isolations better than 30 dB.

ACKNOWLEDGMENT

The authors would like to thank C. Lin from the Avanex Corporation for providing the VIPA samples.

REFERENCES

[1] K. Takada, M. Abe, T. Shibata, and K. Okamoto, "10-GHz-spaced 1010-channel tandem AWG filter consisting of one primary and ten secondary AWGs," *IEEE Photon. Technol. Lett.*, vol. 13, no. 6, pp. 577–578, Jun. 2001.

[2] M. Shirasaki, "Large angular dispersion by a virtually imaged phased array and its application to a wavelength demultiplexer," *Opt. Lett.*, vol. 21, pp. 366–368, 1996.

[3] M. Shirasaki, A. N. Akhter, and C. Lin, "Virtually imaged phased array with graded reflectivity," *IEEE Photon. Technol. Lett.*, vol. 11, no. 11, pp. 1443–1445, Nov. 1997.

[4] T. Yilmaz, C. M. DePriest, T. Turpin, J. H. Abeles, and P. J. Delfyett, "Toward a photonic arbitrary waveform generator using a modelocked external cavity semiconductor laser," *IEEE Photon. Technol. Lett.*, vol. 14, no. 11, pp. 1608–1610, Nov. 2002.

[5] M. Currie, F. K. Fatemi, and J. W. Lou, "Increasing laser repetition rate by spectral elimination," presented at the Conf. Laser and Electro Optics, Baltimore, MD, Jun. 1–6, 2003, Paper CThPDA8.

[6] A. M. Weiner, "Femtosecond pulse shaping using spatial light modulators," *Rev. Sci. Instrum.*, vol. 71, no. 5, pp. 1929–1960, 2000.

[7] M. Shirasaki, "Compensation of chromatic dispersion and dispersion slope using a virtually imaged phased array," presented at the Optical Fiber Communication Conf., Anaheim, CA, Mar. 18–23, 2001, Paper TuS1.

[8] S. Xiao, J. D. McKinney, and A. M. Weiner, "Photonic microwave arbitrary waveform generation using a virtually-imaged phased-array (VIPA) direct space-to-time pulse shaper," *IEEE Photon. Technol. Lett.*, vol. 16, no. 8, pp. 1936–1938, Aug. 2004.

[9] S. Xiao, A. M. Weiner, and C. Lin, "Experimental and theoretical study of hyperfine WDM demultiplexer performance using the virtually-imaged phased-array (VIPA)," *J. Lightw. Technol.*, to be published.

[10] ——, "A dispersion law for virtually-imaged phased-array based on paraxial wave theory," *IEEE J. Quantum Electron.*, vol. 40, no. 4, pp. 420–426, Apr. 2004.